Path instabilities and drag in the settling of single spheres

Facundo Cabrera-Booman [a,b,*], Nicolas Plihon [b], Mickaël Bourgoin [b]

[a] Department of Mechanical and Materials Engineering, Portland State University, Portland, OR, USA
[b] Univ Lyon, ENS de Lyon, CNRS, Laboratoire de Physique, F-69342 Lyon, France

ARTICLE INFO

ABSTRACT

The settling behavior of individual spheres in a quiescent fluid was studied experimentally. The dynamics of the spheres was analyzed in the parameter space of particle-to-fluid density ratio (Γ) and Galileo number (Ga), with $\Gamma \in (1.1, 7.9)$ and Ga $\in (100, 340)$. The experimental results showed for the first time that the mean trajectory angle with the vertical exhibits a complex behavior as Ga and Γ are varied. Numerically predicted regimes such as Vertical Periodic for low Γ values, and Planar Rotating for high Γ values were validated. In particular, for the denser spheres, a clear transition from planar to non-planar trajectories was observed, accompanied by the emergence of semi-helical trajectories corresponding to the Planar Rotating Regime. The spectra of trajectory oscillations were also quantified as a function of Ga, confirming the existence of oblique oscillating regimes at both low and high frequencies. The amplitudes of the perpendicular velocities in these regimes were also quantified and compared with numerical simulations in the literature. The terminal velocity and drag of the spheres were found to depend on the particle-to-fluid density ratio, and correlations between the drag coefficient and particle Reynolds number (Re_p) as a function of Ga were established, allowing for the estimation of drag and settling velocity using Ga, a control parameter, rather than the response parameter Re_p.

1. Introduction

Particles in fluids are representative of many natural and industrial systems and therefore extensively investigated in a variety of scenarios such as turbulence (Cabrera and Cobelli, 2021; Cabrera, 2022; Falkinhoff et al., 2020), and low (Cabrera et al., 2022; Obligado and Bourgoin, 2022) to moderate (Zhou and Dusek, 2015; Jenny et al., 2004) Reynolds number such as this work. Particularly, and despite its apparent simplicity, the physics of finite size spheres settling hides a hierarchy of rich intricate phenomena, some of which are still shrouded in mystery. We are for instance still unable to finely model and predict the terminal velocity of a particle settling in a turbulent environment. The role of linear and non-linear drag (Good et al., 2014; Rosa et al., 2016), the link with possible scenarios enhancing the settling (Maxey, 1987) or hindering it (Nielsen, 1993), the influence of finite size effects (Chouippe and Uhlmann, 2019) and the role of collective effects (Aliseda et al., 2002) are just some examples of subtle couplings which still need to be further explored to improve our capacity to predict the turbulent settling of spherical particles. Challenges are particularly important for environmental issues such as the forecast of particle and pollutants deposition in the atmosphere, rivers and seas.

Interestingly, even the non-turbulent situation, where a sphere settles in a quiescent fluid, is already far from trivial and results in a series of path instabilities (Jenny et al., 2004) not yet understood. These path instabilities are related to a complex wake dynamics which emerges for a sphere with a relative velocity with respect to the surrounding fluid. It is indeed well known for instance that the wake behind a fixed sphere of typical size d, in a steady stream with velocity U and viscosity ν, has a number of bifurcations that depend on Reynolds number Re $= Ud/\nu$. These transitions have been thoroughly explored in numerical and theoretical (Fabre et al., 2008; Tomboulides and Orszag, 2000; Natarajan and Acrivos, 1993) and experimental (Nakamura, 1976; Ormières and Provansal, 1999) studies for the case of fixed spheres in a steady stream for which the onsets of different wake bifurcations are finely characterized.

When the sphere is not fixed (e.g. if it is settling under gravity or rising due to buoyancy in a quiescent fluid), these wake instabilities develop into path instabilities (Ern et al., 2012) as the momentum and torque exerted by the perturbed fluid onto the particle will influence its trajectory. A pioneering work regarding fluidized beds already highlighted the non-applicability of Newton's free settling law on rising particles (Karamanev and Nikolov, 1992), caused by the aforementioned wake effect on the particle trajectory. Jenny and coworkers (Jenny et al., 2003, 2004) made the first systematic numerical study exploring

---

the trajectory dynamics of a single spherical particle settling or rising in a quiescent unconfined fluid. This study was refined later by Zhou and Dusek (2015). The complex dynamics of rising or settling spheres has also been characterized experimentally and theoretically (Bonnefis et al., 2023; Herrada and Eggers, 2023; Auguste and Magnaudet, 2018; Horowitz and Williamson, 2010; Veldhuis and Biesheuvel, 2007; Raaghav et al., 2022).

Two dimensionless numbers control the free sphere settling problem: particle-to-fluid density ratio $\Gamma = \rho_p/\rho_f$ (with ρ_p and ρ_f the particle and fluid densities respectively) and Galileo number $\mathrm{Ga} = \sqrt{|\Gamma - 1|g}d_p^{3/2}/\nu$ (with d_p the particle diameter, g the local acceleration of gravity and ν the kinematic viscosity of the surrounding fluid). The Galileo number was defined here as $\mathrm{Ga} = U_g d_p/\nu$, where the characteristic velocity is the buoyancy velocity $U_g = \sqrt{|\Gamma - 1|g d_p}$. The different regimes and bifurcations of single settling or rising spheres were then assessed in a $\Gamma - \mathrm{Ga}$ parameter space. While the regimes observed for both density ratio below one (rising spheres and bubbles) (Bonnefis et al., 2023; Herrada and Eggers, 2023; Karamanev and Nikolov, 1992; Auguste and Magnaudet, 2018) and for density ratio above unity (particle settling) (Zhou and Dusek, 2015; Horowitz and Williamson, 2010; Veldhuis and Biesheuvel, 2007; Raaghav et al., 2022; Jenny et al., 2004) are interesting, we will restrict ourselves to density ratios larger than unity in the present article. To keep this introduction concise, a detailed review of previous investigations is provided in Section 3, to which our experimental observations are systematically compared. We specifically stress that a number of important regions of the parameter space still remain experimentally unveiled and need to explored in order to characterize the settling regimes and corroborate numerical predictions. This is particularly the case for particle-to-fluid density ratios larger than 3.9 for which no experimental data is available.

Besides the complexity of path instabilities, the drag force experienced by the particles is an important element of the problem which has interested the scientific community. Inquiring in particular on whether the drag force of fixed spheres in a steady stream could be used to estimate the terminal settling or rising velocity of freely moving particles. Raaghav et al. (2022) have studied the drag of rising and settling particles and concluded that for density ratios between 0.86 and 3.9, the particle settling drag estimated from the mean vertical terminal velocity of the spheres does not differ significantly from that of a fixed sphere in free stream flowing at the same velocity. The latter implies that the drag coefficient C_D does not depend on particle-to-fluid density ratio. This idea is used extensively in the literature, and it has been widely used to obtain correlations and empirical models assuming a simple dependency of C_D on particle Reynolds number $\mathrm{Re}_p = v_p d_p/\nu$ (Brown and Lawler, 2003; Tran-Cong et al., 2004). This has been proven incorrect for light particles where a marked dependency appears when $\Gamma < 0.1$ (Karamanev and Nikolov, 1992; Auguste and Magnaudet, 2018).

Another practical issue is that the correlations for drag and settling velocity available in the literature are usually given in terms of the particle Reynolds number. However, when the particles are free to move, the velocity v_p is not a control parameter but a response parameter. For the case of settling particles, these correlations do not allow to give an explicit expression for the terminal velocity in terms of the drag coefficient C_D, because C_D itself depends on the terminal velocity. However, from a pure dimensional analysis approach, the natural expected dependencies of the drag coefficient for settling spheres are both on Γ and Ga, which are actual control parameters, only depending on known physical parameter of the problem (densities of the particles and the fluid, fluid viscosity, particle diameter and acceleration of gravity). This brings the two following questions: (i) to which extent is the approximation of C_D not depending on density ratio valid? And (ii) can a correlation of C_D be given in terms of Ga rather than Re_p? This would allow to know the drag coefficient *a priori* without requiring to know the terminal velocity beforehand.
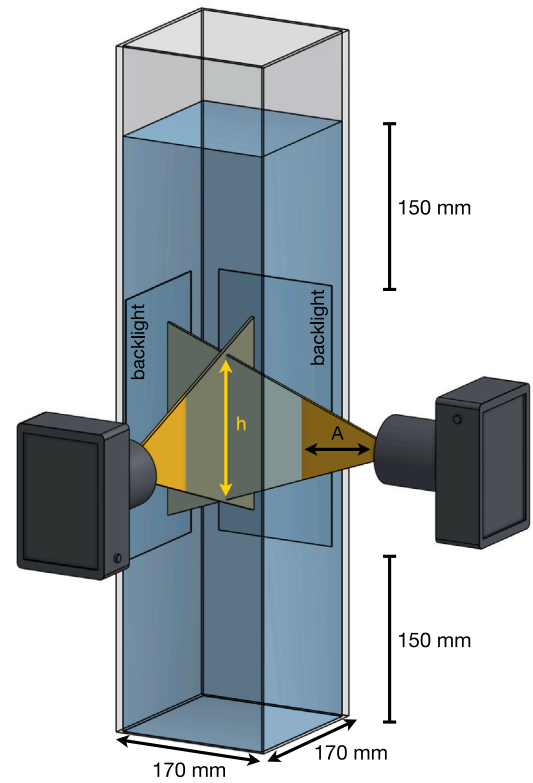

Fig. 1. Experimental setup. Two cameras image the particles settling inside the water tank. (For interpretation of the references to color in this figure legend, the reader is referred to the web version of this article.)

In the present article, we investigate experimentally the settling of spherical particles in a quiescent fluid over a broad region of the parameter space, namely $1 < \Gamma < 8$ and $100 < \mathrm{Ga} < 350$ (symbols in Fig. 2 indicate all points explored in the parameter space). For all the investigated conditions, we fully characterize the trajectory properties of the particles as well as the drag coefficient derived from the particle's terminal velocity. The article is organized as follows. We first introduce the experimental setup in Section 2. The results are then described in Section 3. Finally, our conclusions are summarized in Section 4.

2. Experimental methods

2.1. Experimental setup and protocol

The experiments are performed in a transparent PMMA tank with a square cross-section of 170×170 mm^2 and a height of 710 mm, shown in Fig. 1. The tank is filled with different mixtures of pure glycerol (Sigma-Aldrich W252506-25KG-K) and distilled water, ranging from 0% to 40% glycerol concentration. The viscosity of each mixture is measured with a rheometer Kinexus ultra+ from Malvern industries with a maximum uncertainty of 0.6%. The kinematic viscosity ν ranges from 10^{-6} to 1.05×10^{-3} m^2/s. Moreover, as the viscosity is dependent on the temperature, an air-conditioning system keeps a constant room temperature of (22 ± 0.6) °C yielding a 2% uncertainty on the precise value of the viscosity.

A 150 mm region of fluid above and below the visualization volume is set to ensure both the disappearance of any initial condition imposed on the particles release and the effects of the bottom of the tank. Furthermore, a minimum distance of 20 mm between the tank walls and the particles is maintained. In this configuration and using the correlations proposed by Chhabra et al. (2003) the settling velocity hindering due to wall effects is estimated to be lower than 3%.
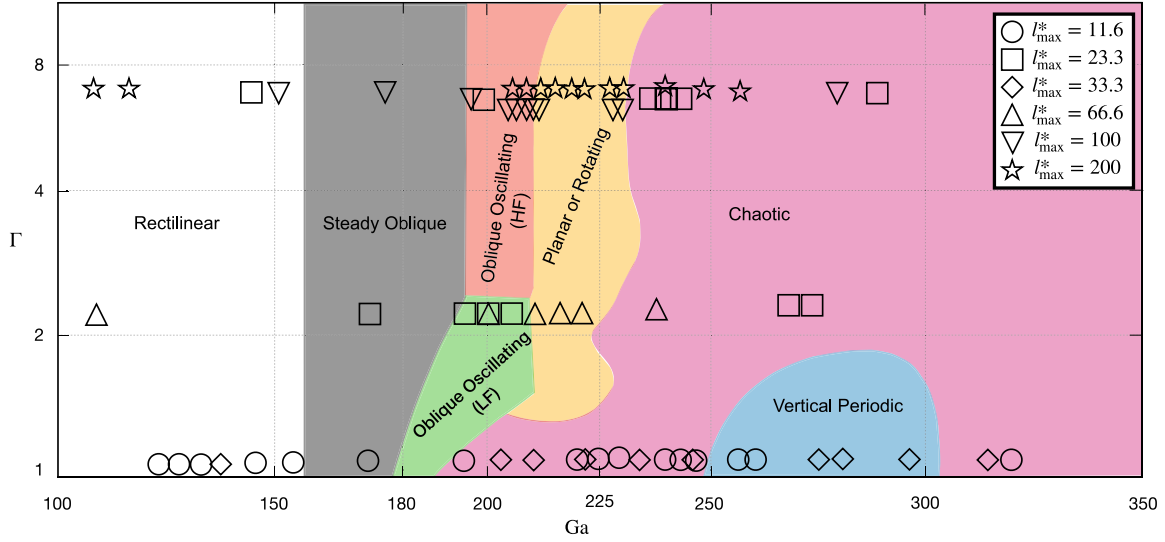
Fig. 2. Particle-to-fluid density ratio (Γ) – Galileo number (Ga) space of parameters. Data points are classified by their maximum trajectory length $l^*_{max} = h/d_p$. (For interpretation of the references to color in this figure legend, the reader is referred to the web version of this article.)

The trajectory of the settling particles is recorded using two high speed cameras (model fps 1000 from The Slow Motion Camera Company *Ltd*) with a resolution of 720×1280 px^2 and a frame rate of 2300 fps. The movies recorded from these two cameras allow the implementation of time resolved 4D-Lagrangian Particle Tracking (4D-LPT) to reconstruct the particle trajectories (Bourgoin and Huisman, 2020). This method tracks particles with an uncertainty of 90 μm which is estimated from the disparity between rays when stereo-matching the particle between the two cameras. This experimental noise on the particle position is short time correlated and gets significantly reduced by the high temporal redundancy associated to the oversampling achieved with the frame rate of 2300 Hz and the subsequent gaussian filtering of the trajectories (further detailed below) used to estimate particle velocity. As a consequence, the uncertainty on the instantaneous velocity along trajectories is less than 4 mm/s (Bourgoin and Huisman, 2020) while the associated uncertainty for the velocity averaged over a given trajectory drops below a few hundred microns per second. Backlight illumination was used, with two LED panels facing each camera on the opposite side of the tank, as represented by the dark blue rectangles in Fig. 1.

Various series of experiments were carried with different optical magnification ratios, in order to access large scale properties of the trajectories (with lower magnification) as well as higher resolution data (with higher magnification). The magnification was varied by keeping the same optics mounted on the cameras, and varying the distance A from the cameras to the exterior of the tank's wall. The datasets corresponding to these different situations are detailed in the next subsection.

In order to span the Γ - Ga parameters space, we considered a set of spherical particles with different diameters (d_p) and densities (ρ_p), while varying the water-glycerol mixture in order to vary the fluid viscosity ν. Varying the fluid viscosity ν allows to change Ga for a given type of particle, at the expense of the slight modification of the value of Γ due to the associated variation of the fluid density. The characteristics of the particles and the ranges of values Ga and Γ investigated in this articles are reported in Table 1. Overall, a total of 68 points in the Γ - Ga parameters space has been explored (see Fig. 2). For each point up to 25 independent drops were released in order to test the repeatability of the observed regimes and the eventual presence of bi-stable regions where different settling regimes could co-exist in the same region of the parameters space. The particle's diameter and sphericity were measured using a microscope with a precision of 10 μm.

Table 1
Properties of the different settling particles investigated. See text for details.

Material (label)	ρ_p (kg/m^3)	d_p (mm)	Γ	Ga	Ra (μm)
Metal	7950	{1, 2, 3}	6.6–7.8	112–290	9
Glass	2500	3	2.1–2.5	130–270	15
Polyamide	1150	6	1.1–1.3	124–340	120

In particular, no significant deviation from the spherical shape or the manufacturer's documented diameter could be measured. The surface roughness of the particles was also measured, with a Scanning Electron Microscope ZEISS SUPRA 55 VP, over an area of 200×500 μm^2. The arithmetical mean height of rugosities Ra reported in Table 1 shows a high degree of smoothness as Ra/$d_p < 0.05$, therefore roughness is not expected to alter the spheres dynamics (Zhao and Davis, 2003). In particular, the following particles were used: Metal - *Stainless Steel Ball AISI 316 Grade 100* from COMAC Europe; Glass - *Soda Lime Grade 60* and Polyamide - *PA 6.6 Grade 2* both from Marteau & Lemarié.

The experimental procedure is the following: the tank is filled with a water-glycerol mixture and after approximately 24 h the temperature at different positions in the fluid's bulk differs in less than 0.6 °C thus thermal equilibrium is reached. Then a standard calibration of the 4D-LPT system is performed (Bourgoin and Huisman, 2020). The spheres are released at the center of the tank with standard Stainless Steel Anti-acid and Anti-magnetic chemical tweezers. The tweezers are completely submerged below the air–liquid interface and released after approximately 20 s when the fluid free surface is at rest. A minimum time of 120 s is taken between successive drops to ensure that the fluid has no perturbations left from the previous drop. The waiting time is chosen to be at least 12 viscous relaxation times $\tau = d_p^2/\nu$. Note that the viscous times vary between different cases and the resulting waiting time is in between 12τ and 1000τ, with a median value of 150τ.

2.2. Data sets

The experiments were conducted using two different optical magnifications, resulting in various values of the non-dimensional trajectory length $l^*_{max} = h/d_p$ ranging from 11.6 to 200 (see Fig. 1). Note that the lowest values of l^*_{max} (11.6 and 23.3) correspond to the larger optical magnification, or small A (hence giving better spatial resolution, but shorter tracks) while the larger values of l^*_{max} were obtained with the smaller magnification, or large A (resulting in a larger field of

view, hence giving access to longer trajectories, what is important in particular to properly estimate the frequency of oscillating regimes). The values of $l^*_{\max}$ are reported in the $\Gamma - $ Ga parameters space in Fig. 2.

All the relevant geometric (inclination and planarity) and dynamic characteristics (spectral content and terminal velocity) of particle trajectories cannot be equally addressed from the different datasets as the accuracy of their estimate depends on the maximum accessible track length $l^*_{\max}$. Empirically, we found that to reasonably resolve trajectory inclination, a dimensionless trajectory length of at least $l^* \gtrsim 10$ (which is accessible with all datasets) is needed. This has been tested by checking the estimation of the inclination angle using the longest trajectories in the oblique regime and successively considering shorter and shorter portions of those long tracks. On the other hand, the quantification of the planarity via the eigenvalue method detailed in Section 3, requires $l^* \gtrsim 23$ - a condition not met for plastic particles, due to their large diameter. This conclusion has been reached by checking the estimation of the planarity using the longest available trajectories in the chaotic regime and successively considering shorter and shorter portions of those long tracks. This effect will be explored further in Section 3.3. Finally, the spectral analysis required long trajectories, an issue further discussed in Section 3.4.

In order to reduce experimental noise (due to inevitable particle detection errors in the Lagrangian Particle Tracking treatment Ouellette et al., 2005), the raw trajectories are smoothed by convolution with a Gaussian kernel of width $\sigma = 12$ frames. It behaves as a low-pass filter with a cut-off frequency $f_c = $ fps$/\sigma = 2300$ Hz$/\sigma = 192$ Hz. Spectral analysis is therefore expected to be well resolved for frequencies up to of the order of 80 Hz as to respect the Nyquist–Shannon sampling theorem.

As previously mentioned, for each data point in the Γ - Ga parameters space, at least 10 and up to 25 experimental repetitions were executed and their trajectories analyzed. This is mandatory in order to test the repeatability of the observed regimes, estimate uncertainties, and eventually detect multi-stable regions of the parameters space where multiple settling regimes may coexist. The uncertainties in quantities extracted from this data (e.g. trajectory angle or planarity) are taken as the standard deviation over the total set of drops for each data point. For computed quantities (i.e. Reynolds number, Galileo number and Drag coefficient) the errors are estimated from a standard propagation of errors, see for instance Raaghav et al. (2022).

Finally, in the remainder of this article, dimensionless parameters are denoted by a superscript asterisk. Spatial variables are normalized by particle diameter $x^* = x/d_p$, velocities are normalized by the buoyancy velocity $v^* = v/U_g = v/\sqrt{|\Gamma - 1|g d_p}$, and time is normalized by the response time of the particles $\tau_g = d_p/U_g$.

3. Results

In this section, we first recall and present the different settling regimes reported in the literature. Then, the features of the 68 points experimentally investigated in the parameter space (Fig. 2) are described. Particular emphasis is put on their geometric and spectral properties, as well their terminal velocity and drag coefficient estimation

3.1. Different regimes

The different regimes in the parameters space obtained from numerical simulations by Zhou and Dusek (2015) are represented by different colors in Fig. 2. Seven distinct regimes were numerically identified, whose features are summarized in the following:

1. Rectilinear Regime (white), with planar vertical trajectories and no inclination or oscillations;
2. Steady Oblique Regime (gray), with planar and oblique trajectories with respect to the vertical, and no oscillations;

3. Oblique Oscillating Regime, with planar and oblique trajectories, and the presence of oscillations. The frequency of oscillations f^* depends on the particle–fluid density ratio Γ, with a High-Frequency Regime (HF, orange) at $f^* \simeq 0.18$ and a Low-Frequency (LF, green) at $f^* \simeq 0.068$.
4. Planar or Rotating Regime (yellow), a bi-stable region of the parameters space composed of oblique and (High or Low-Frequency) oscillating trajectories, which could be either planar or exhibit a slowly rotating symmetry plane (thus generating helicoid-like trajectories), coexisting with Chaotic Regimes. The High-Frequency Regime, Low-Frequency Regime, and Chaotic Regime coexist in this zone.
5. Vertical Periodic Regime (blue), where the trajectories are planar, rectilinear and vertical, and oscillate at $f^* \in (0.141, 0.15)$;
6. and finally the Chaotic Regime (pink), with oblique and non-planar trajectories with no periodic oscillations.

A systematic study of the bifurcations between regimes was performed numerically by Zhou and Dusek (2015). That study narrowed down the limits between regimes, in terms of Ga and Γ, and has reported new regimes not previously detected in the simulations by Jenny et al. (2003, 2004) (such as a Helical/Rotating Regime and a Vertical Periodic Regime). They also demonstrate the existence of bistable zone in the parameters space, where two regimes could co-exist. For instance, for moderate particle-to-fluid density ratios $\Gamma \lesssim 2$ a bistable regime between a Chaotic and a Vertical Oscillating Regime are reported, while for larger density ratios they report bi-stability between Planar Oscillating and Helical Regimes. Furthermore, they have better quantified trajectory parameters such as angle, velocities and spectral content. Note that this description of the dynamics of individual particles was later used as a benchmark for numerical investigations of collective particle effects (Uhlmann and Doychev, 2014; Fornari et al., 2016). Few analytical results have been derived regarding the bifurcations between different settling regimes, one exception being the transition between the Rectilinear and the Steady Oblique Regimes which have been analytically shown by Fabre et al. (2012) to occur at a critical Galileo number of the order of 155, independently of the particle-to-fluid density ratio, in excellent agreement with the numerical findings previously mentioned.

To the best of our knowledge, only three experimental studies (Veldhuis and Biesheuvel, 2007; Horowitz and Williamson, 2010; Raaghav et al., 2022) have explored the predictions made by aforementioned simulations and theories. Horowitz and Williamson (2010) were mostly interested in regimes for rising spheres or slightly denser than the fluid and high Galileo numbers: they studied particle-to-fluid density ratios Γ below 1.4 and Galileo numbers ranging from 10^2 to 10^4. In particular, they studied trajectory angle and drag following the work of Karamanev and Nikolov (1992). Intriguingly, most findings from this study deviate from numerical simulations by Zhou and Dusek (2015), in particular for the case of settling particles which will be investigated here. On the other hand, Veldhuis and Biesheuvel (2007), although with some discrepancies, observed several of the dynamical regimes observed in the numerical simulations. In particular, oblique trajectories with no significant frequencies (Steady Oblique Regime in simulations) were reported. They also report oblique trajectories with oscillations at three dominant dimensionless frequencies of 0.07, 0.017 and 0.025 (Oblique Oscillating Regime in simulations), whose presence depends on the particle-to-fluid density ratio Γ. Finally, an oblique chaotic regime with no dominant frequencies and random trajectory curvature (Chaotic Regime) was described. These regimes were measured for particle-to-fluid density ratios Γ of 1.3 and 2.3 at various Galileo numbers spanned by varying the fluid viscosity. Finally, in 2022, Raaghav et al. (2022) performed experiments on rising and settling particles, with four particle-to-fluid density ratios ($\Gamma = 0.87$, 1.12, 3.19 and 3.9) and Ga ranging from 100 to 700. They confirmed and contradicted some results of previous numerical simulations and
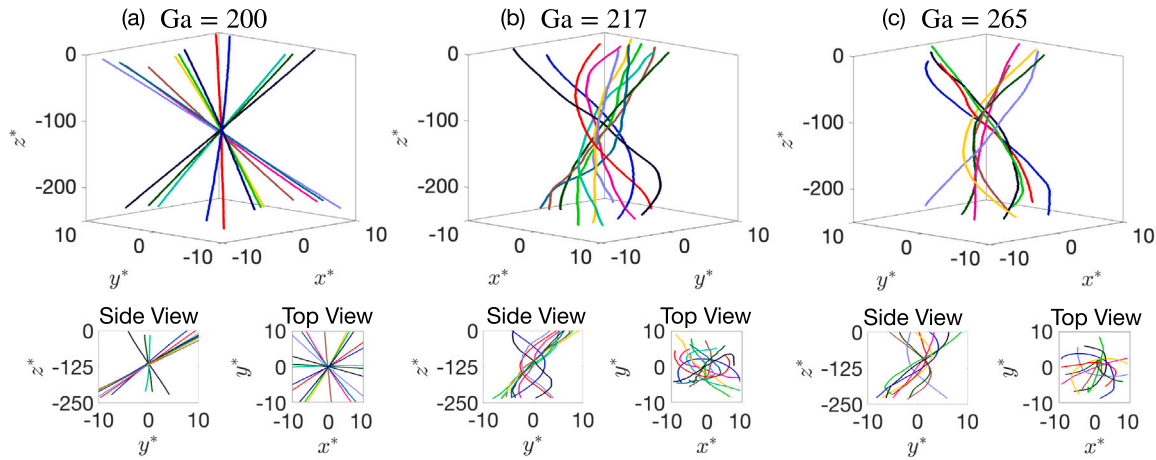
Fig. 3. Typical trajectories for particles with $\Gamma \approx 7.9$ in the: (a) Steady Oblique; (b) Planar or Rotating; and (c) Chaotic Regimes. (For interpretation of the references to color in this figure legend, the reader is referred to the web version of this article.)

experiments. The low Ga regimes (up to the Steady Oblique Regime) is unambiguously confirmed, in agreement with previous studies. For higher Galileo numbers (typically above 200), they found however discrepancies both with previous numerical and experimental studies. For instance, they observed a bi-stable behavior (between the Oscillating and Chaotic Regimes) for moderately dense spheres ($\Gamma \simeq 1.1$) in the range $250 < Ga < 300$ in agreement with by Zhou and Dusek (2015), but for density ratios above 3, they did not observe the High-Frequency Oblique Oscillating Regime reported by Zhou and Dusek (2015); they confirmed though the existence of a helical mode, although no bi-stability with the Chaotic Regime was observed, contrary to the findings by Zhou and Dusek (2015) reported.

Our experiments confirm the existence of all the predicted regimes, in regions of the parameters space in relatively good agreement with the ones delimited by numerical simulations. Fig. 3(a–c) qualitatively show some examples of trajectories. More specifically, Fig. 3(a–c) show some representative 3D trajectories for $\Gamma \approx 7.9$ particles, from the $l^*_{max} = 200$ dataset. The trajectories have been arbitrarily centered in the horizontal axis. Sub-figures show top and side views.

Fig. 3(a) represents a case of planar and oblique type of trajectories measured here at Ga = 200. Note that steady and oscillating regimes are almost indistinguishable in such a representation by a simple visual inspection of the trajectories as the amplitude of oscillations is of the order of the particle diameter. The distinction between the two regimes will be quantitatively discussed later, based on the estimation of the particle velocity and their spectral analysis (the example shown in Fig. 3(a) is actually an oblique oscillating case). It can also be noted that the angle of the trajectories with the vertical in this oblique regime remains almost constant for all drops (the angle will be quantitatively investigated in the next subsection, and is of the order of 5° in the present example), but each trajectory has its own direction so that the ensemble forms a cone hence preserving the global symmetry of the problem.

Fig. 3(b) represents a sample of trajectories of $\Gamma \approx 7.9$ particles at Ga = 217. By combining the side and top views, it can be seen that several of these trajectories are consistent with portions of helicoids (for instance the red and the dark blue curves, which appears as quasi circular from the top view, although even with the $l^*_{max} = 200$ dataset, we only catch half of the period at most). Those co-exist with non-planar chaotic trajectories (as for instance the black and yellow curves). These measurements fall in the tri-stable regime previously mentioned.

Finally, Fig. 3(c) presents several trajectories that fall in the Chaotic Regime: all trajectories are different and no pattern of planarity or oscillations is present.

After this brief qualitative description of some observed trajectory regimes, the next Subsections present a systematic quantitative analysis
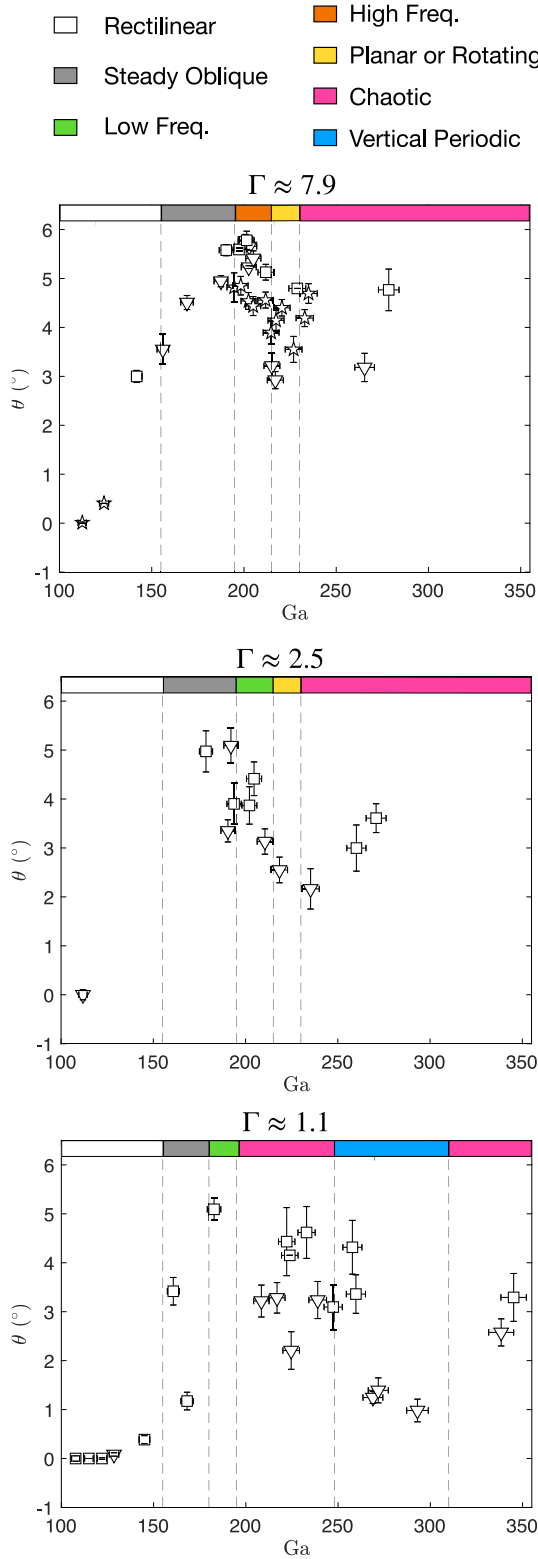
of the different properties used to characterize trajectory geometry and dynamics: angle with the vertical, planarity, spectral content, terminal velocity, and drag.

3.2. Trajectories angle

For each recorded trajectory we define the settling orientation as the angle between a 3D linear fit of the trajectory and the vertical, and for each given set of parameters (Ga, Γ) we define the mean settling orientation as the ensemble average of settling angles over all trajectories recorded at those parameters. Fig. 4 shows the mean settling orientation as a function of Ga for the three different classes of particles investigated ($\Gamma \approx 7.9$, $\Gamma \approx 2.5$ and $\Gamma \approx 1.1$). Besides, the different settling regimes as reported from numerical simulations and previously shown in Fig. 2 are delimited by the dashed vertical lines and identified by colored rectangles that respect the color code in Fig. 2. Furthermore, the type of symbols represents the value l^*_{max}, also following the nomenclature of Fig. 2.

A smooth transition from rectilinear to oblique (primary regular bifurcation) is seen around the expected critical Galileo number of 150 for $\Gamma \approx 1.1$ and $\Gamma \approx 7.9$ particles and, although there is a lack of data points in this region of Ga for $\Gamma \approx 2.5$ particles, the available data points are consistent with a similar transition also occurring in the same range of Ga for those particles. More precisely, if the threshold between this regimes is defined as the Galileo number value at which the angle of the mean settling orientation has a non-zero angle, $\Gamma \approx 1.1$ and $\Gamma \approx 7.9$ particles present threshold values of (125 ± 10) and (115 ± 10) respectively, leading to a joint threshold at Ga = (120 ± 15). The trajectory angle is then found to continuously vary with the Galileo number; see for example $\Gamma \approx 7.9$ particles: the angle varies monotonously from 0 to 6 degrees in the Ga range 110–190. With this respect, the transition between the rectilinear regime and the steady oblique regime in our experiment somewhat appears as an imperfect bifurcation rather than a sharp bifurcation with a critical Galileo number $Ga \approx 155$. The origin of such an imperfect bifurcation remains unclear and would deserve further future investigations.

Additionally, the maximum observed angles are $(5.7° \pm 0.2°)$, $(5.1° \pm 0.2°)$ and $(5.1° \pm 0.2°)$ for density ratios 7.9, 2.5 and 1.1, respectively. This maximum angle is reached around Ga = 200 in all cases in the region of parameters space that has been identified in numerical simulations by Zhou and Dusek (2015) and previous experiments (Horowitz and Williamson, 2010; Raaghav et al., 2022) as corresponding to the Oblique Regimes, although the distinction between steady and oscillating regimes requires further analysis of the spectral content of the trajectories, which will be presented later. We note also that, although

Fig. 4. Trajectory angle versus Galileo number for the three particle densities. Regimes are delimited by dashed vertical lines and identified by colors following Fig. 2. Symbols represent the value of l_{max}^*, according to Fig. 2. (For interpretation of the references to color in this figure legend, the reader is referred to the web version of this article.)

the range of angles previously reported: "of about 4 to 6 degrees" in the Steady Oblique and Oblique Oscillating Regimes in numerical simulations by Zhou and Dusek (2015), "approximately 4° to 7.5°" in Horowitz and Williamson (2010) and "approximately 2.8° to 7.4°" in Raaghav et al. (2022).

It can be seen in Fig. 4 that for large Galileo numbers (typically Ga > 200) multiple values of the average settling angle can be observed for similar values of Ga. These situations are generally consistent with regions of the parameters space which have been identified in numerical simulations either as multi-stable (yellow) or chaotic (pink). For the denser particles, such multi-values of the settling angle are for instance pronounced in the range Ga ∈ (200, 230) encompassing both the HF-Oblique Oscillating (orange) and tri-stable Planar/Rotating (yellow) regions of the numerical parameters space, what may suggest that the multi-stable Planar/Rotating Regime, identified numerically around Ga ≈ 220, may actually extend further into the HF-Oblique Oscillating region at lower Galileo numbers. For the lightest particles, the trend to observe multiple values of the settling angle is very clear in regions of Ga expected to correspond to the Chaotic Regime (pink), in particular in the range Ga ∈ (200, 260). For the intermediate density case ($\Gamma \approx 2.5$), this trend is observed in the vicinity of the LF-Oblique Oscillating Regime (green), what may be a sign that as for the dense particles case, the region numerically identified as bi-stable Planar/Rotating (yellow) may actually extend to lower values of Ga particularly into the LF-Oblique Oscillating region.

It is also interesting to see that for the $\Gamma \approx 1.1$ particles the drop of the settling angle in the range Ga ∈ (250, 300) is consistent with the numerical prediction of a Vertical Periodic Regime (blue) appearing in that range and surrounded by Chaotic Regimes.

Overall, measured settling angles are consistent with what is expected from the numerical parameters space. With the exception of a probably more extended multi-stable region (yellow) overlapping (partially or totally) the Oblique-Oscillating regions.

3.3. Trajectories planarity

The trajectory planarity is quantified by the ratio of eigenvalues λ_2/λ_1 (with $\lambda_1 \geq \lambda_2$) of the dimensionless perpendicular (to gravity) velocity correlation matrix defined as:

$$\langle \mathbf{v}_\perp^* \ \mathbf{v}_\perp^{*T} \rangle = \begin{bmatrix} \langle v_x^{*2} \rangle & \langle v_x^* v_y^* \rangle \\ \langle v_y^* v_x^* \rangle & \langle v_y^{*2} \rangle \end{bmatrix}, \tag{1}$$

with $v^* = v/U_g$. Perfectly planar trajectories yield $\lambda_2/\lambda_1 = 0$, while non-vanishing values of this ratio indicate a departure from planarity (Zhou, 2016). Note that the analysis of the planarity only yields meaningful results for trajectories with $l_{max}^* > 33.3$. Fig. 5 shows the ratio $\sqrt{\lambda_2/\lambda_1}$ versus Ga number, for the three types of particles. As in previous figures, the different regimes are delimited by dashed vertical lines and identified by colored rectangles.

Planarity is lost at Ga = (220 ± 15) for $\Gamma \approx 7.9$ particles and at Ga = (220 ± 15) for $\Gamma \approx 2.5$ particles. At these points the ratio between the eigenvectors of the velocity correlation matrix $\sqrt{\lambda_2/\lambda_1}$ increases from approximately 0.15 to 0.50 for $\Gamma \approx 7.9$ particles (0.30 for $\Gamma \approx 2.5$ particles). The range of Galileo number where planarity is found to be lost is consistent with the transition towards the Planar or Rotating Regime reported in numerical simulations by Zhou and Dusek (2015), with a possible overlap with the LF-Oblique Oscillating region for $\Gamma \approx 1.1$ particles and with the HF-Oblique Oscillating region for $\Gamma \approx 2.5$ particles. On the other hand, no clear transition between planar and non-planar trajectories is observed for $\Gamma \approx 1.1$ particles, which may be due to too small values of l_{max}^*.

In the case of $\Gamma \approx 7.9$ particles, the loss of planarity seems to be associated to the emergence of helicoidal trajectories. Fig. 3(b) presents indeed a sample of trajectories for $\Gamma \approx 7.9$ particles, representative of the ensemble of trajectories at Ga ∼ 217, that are consistent with a half-helicoid. Similar trajectories are found at Ga = {215, 217, 221}

the detailed trend of the settling angle with Ga as presented here has not been systematically explored in previous studies, the values we observe for the maximum settling angle are in good agreement with
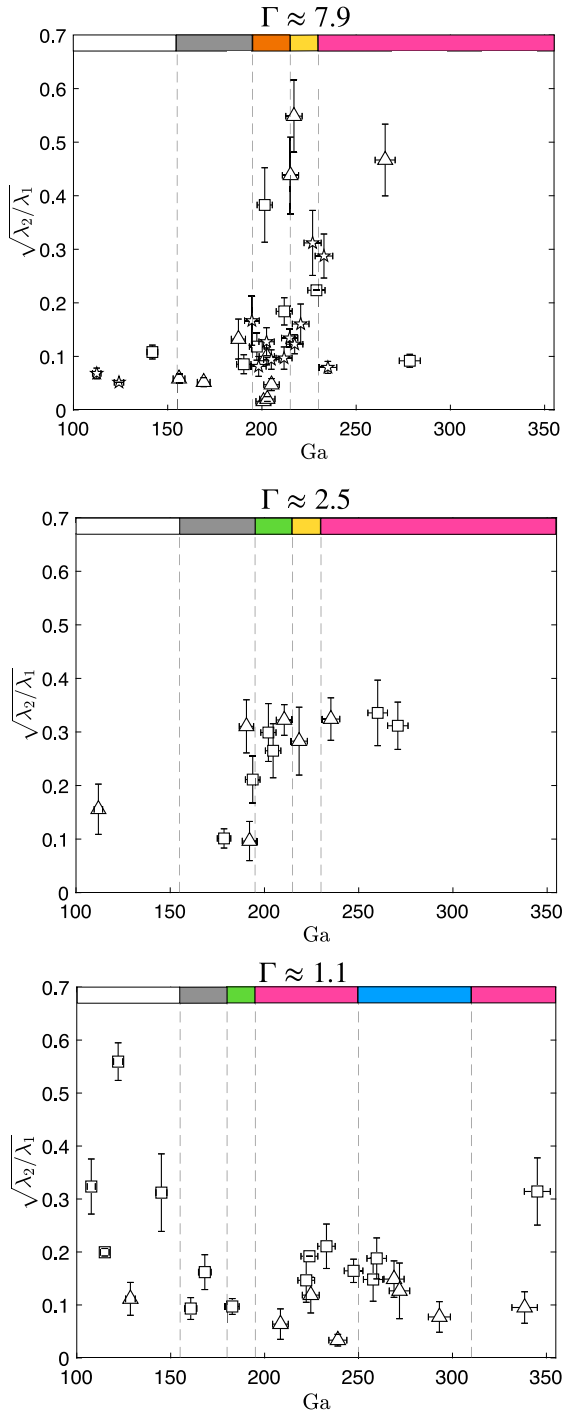
Fig. 5. Planarity versus Galileo number for the three particle densities. Regimes are delimited by dashed vertical lines and identified by colors following Fig. 2. Symbols represent the value of l^*_{max}, according to Fig. 2. (For interpretation of the references to color in this figure legend, the reader is referred to the web version of this article.)

and Ga = {228,233}, for several values of $l^*_{max} > 33.3$. Hence the aforementioned loss of planarity for data with Galileo numbers larger than (220 ± 15) (see Fig. 5) can be related to the appearance of these helicoid-like trajectories. Limitations of the measurement volume, even in the $l^*_{max} = 200$ configuration, do not allow to be fully conclusive as only a portion of the helicoid's period is recognizable. However, assuming that these trajectories are helicoids, the radius of their horizontal projection (Fig. 3(b) top view) would be roughly 7 particle diameters,

and their pitch would be approximately 500 particle diameters. Similar helicoid-like trajectories have also been seen experimentally in previous studies, although for smaller density ratios, $\Gamma < 3.9$ (recall that metallic particles in the present study have a density ratio $\Gamma \simeq 7.5$, which has not been investigated in previous works): Veldhuis and Biesheuvel (2007) reported what are possibly helicoidal trajectories for particles with density ratio of the order of $\Gamma \simeq 2.5$ (hence close to the present $\Gamma \approx 2.5$ particles), while Raaghav et al. (2022) found similar trajectories for particles with $\Gamma = \{3.2, 3.9\}$. Their results show a pitch of the order of 430 d_p which is comparable to the one of 500 d_p found here. In this sense, the results of this work confirm the existence of such non-planar, very likely helicoidal, regime for Ga $\in (215, 233)$ at larger particle-to-fluid density ratios, in the range of metallic particles ($\Gamma \approx 7.9$). Recall that the short l^* in the data sets of $\Gamma \approx 2.5$ and $\Gamma \approx 7.9$ particles do not allow to see a portion of an helicoid long enough to make such claims.

Fig. 5 for $\Gamma \approx 2.5$ an $\Gamma \approx 7.9$ particles also shows signatures of non-planarity in the region numerically identified as chaotic (Ga $\gtrsim$ 230), in agreement with the sample trajectories shown in Fig. 3(c), where several trajectories show a clear departure from simple portions of helicoids. A clear distinction between non-planar helicoidal and chaotic trajectories, with a systematic characterization of the pitch and radius of the helicoids and of the frontier with the Chaotic Regime would nevertheless require further dedicated experiments with a taller visualization volume.

3.4. Trajectories oscillations

We analyze the emergence of oscillatory dynamics by studying the fluctuations of the horizontal (*i.e.* perpendicular to gravity) dimensionless velocity: $v'^*_\perp := v^*_\perp - \langle v^*_\perp \rangle$. In particular, while oblique-oscillatory regimes have been experimentally reported for density ratios below 3.9, we want to confirm here their existence at higher density ratios (*i.e.* for the $\Gamma \approx 7.9$ particles, with $\Gamma = 7.9$) and in that case evaluate the corresponding frequency. On the other hand, the existence of a Vertical Periodic Regime (light blue region in Fig. 2) for density ratios below 1.8, as predicted by Zhou and Dusek (2015) was only very recently corroborated experimentally (Raaghav et al., 2022). This regime is expected to have trajectories with zero angle and Low-Frequency Oscillations. Recall that the regime has been already discussed in the previous section where a sharp decrease in trajectory angle was found. We will therefore confirm here that the oscillations are at the Low-Frequency $f^* \approx 0.06$.

Numerical simulations by Zhou and Dusek (2015) predict the existence of Oblique-Oscillatory Regimes for Ga of the order of 200, with a characteristic dimensionless frequency f^* which depends on the density ratio Γ. More specifically, the simulations by Zhou and Dusek (2015) predict a transition from a Low-Frequency Regime (with a dominant dimensionless frequency $f^* \approx 0.07$, corresponding to green regimes in previous graphs) to a High-Frequency Regime (with $f^* \approx 0.18$, corresponding to orange regimes in previous graphs) occurring at $\Gamma \approx 2.3$. However, previous experiments by Veldhuis and Biesheuvel (2007) and Raaghav et al. have only partially confirmed this scenario. Veldhuis and Biesheuvel (2007) for instance did observe Oblique-Oscillating Regimes in the expected range of Galileo number for particles with density ratios $\Gamma \approx 1.5$ and $\Gamma \approx 2.5$, but they report a dominant characteristic frequency of $f^* \approx 0.25$ for the lower density ratio case (*i.e.* about three times higher than the numerical prediction) while two main frequencies, of the order of 0.07 and 0.25, were detected for the larger density ratio. On the other hand, Raaghav et al. consistently report a Low-Frequency Oblique-Oscillating Regime (with $f^* \approx 0.06$) for particles with density ratio $\Gamma \approx 1.1$, but did not find any planar High-Frequency Oblique-Oscillating Regime for particles with $\Gamma = 3.9$, for which only non-planar helical trajectories (similar to those reported in the previous section of this work) were observed. The existence of Oblique-Oscillating Regimes (and eventually the value of their frequency) for high density ratios therefore remains open.
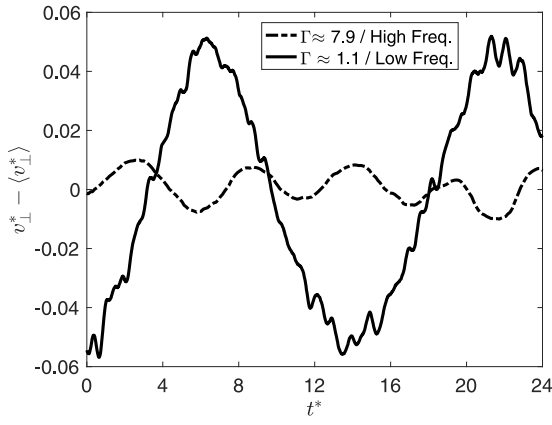
Fig. 6. Typical perpendicular (to gravity) velocity fluctuations for particles with $\Gamma \approx 1.1$ and Ga = 208 that correspond to the Low-Frequency Regime (continuous line), and particles with $\Gamma \approx 7.9$ and Ga = 200 in the High-Frequency Regime (dashed line).
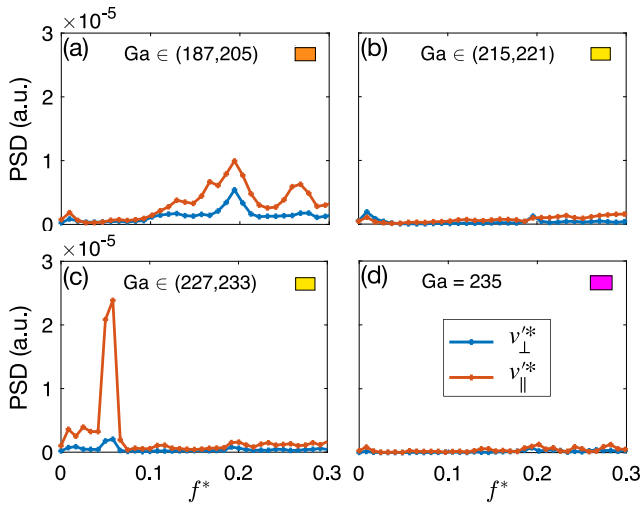

Fig. 7. PSD of parallel and perpendicular dimensionless velocity fluctuations ($v'^{*}_{\parallel}$ and $v'^{*}_{\perp}$, respectively) for $\Gamma \approx 7.9$ particles. Colors correspond to Regimes defined in Fig. 2.

Fig. 6, shows a sample of perpendicular velocity fluctuations versus time for $\Gamma \approx 7.9$ particles at Ga = 200, and $\Gamma \approx 1.1$ particles for Ga = 208. They exhibit a clear oscillatory dynamics, which is oblique (remember that $\theta \approx 5°$ for particles at these Ga) with marked frequency and amplitude differences. $\Gamma \approx 7.9$ particles show higher frequency and smaller amplitude than $\Gamma \approx 1.1$ particles. These observations are in qualitative agreement with numerical predictions. The amplitude ratio between the High and Low-Frequency perpendicular dimensionless velocity oscillations of approximately 5 times is found however to be substantially smaller than what is reported in numerical simulations by Zhou and Dusek (2015) where a ratio of 12 is observed. From the oscillations reported in Fig. 6, it is possible to estimate the typical dimensionless frequencies f^{*} for both regimes which is found to be of the order of 0.07 for the Low-Frequency case ($\Gamma \approx 1.1$ particles) and of the order of 0.2 for the High-Frequency case ($\Gamma \approx 7.9$ particles). These values are in good agreement with the numerical prediction, and the spectral analysis that follows.

A more accurate and systematic analysis of the oscillatory dynamics in the different regimes can be performed by computing the Power Spectral Density (PSD) of the velocity fluctuations averaged over multiple realizations in a narrow range of Ga. Fig. 7 presents various PSD of velocity fluctuations at different values of the Galileo number, for the $l^{*}_{max} = 200$ data-set of $\Gamma \approx 7.9$ particles. Both parallel and

perpendicular components of velocity fluctuations have been analyzed. Each sub-figure presents the ensemble average of all PSDs in ranges of Ga where the spectral content was found to be robust: Ga = {187, 195, 198, 202, 205} for Fig. 7(a), Ga = {215, 217, 221} for Fig. 7(b), Ga = {227, 233} for Fig. 7(c), and Ga = 235 for Fig. 7(d). We note that the spectral resolution, limited by the accessible trajectory length, is 0.01. All measurements with Ga smaller than 187 have no spectral content (settling is then stationary, either vertical or oblique), therefore not shown.

The perpendicular velocity fluctuations PSDs presented in Fig. 7(a) show that for Ga $\in (187, 205)$ oscillations have a broad frequency peak centered around a dominant frequency $f^{*} = (0.19 \pm 0.01)$, and a secondary frequency around $f^{*} = (0.27 \pm 0.01)$. The dominant frequency confirms the High-Frequency nature of the oscillations qualitatively discussed in the previous paragraphs for $\Gamma \approx 7.9$ particles at Ga = 200, corresponding to the perpendicular velocity signal shown in Fig. 6. It is also in agreement with the frequency predicted in numerical simulations by Zhou and Dusek (2015) for such dense particles in this range of Galileo number, where a High-Frequency Oblique Oscillating Regime, with $f^{*} = 0.18$ has been reported by Zhou and Dusek (2015).

The main difference between these experiments and the simulations by Zhou and Dusek (2015) is the non-negligible intensity of the peak at $f^{*} \approx 0.27$ (and possibly a sub-harmonic of $f^{*} \approx 0.13$). The existence of the frequency peak at $f^{*} = 0.27$ reminds of the observation by Veldhuis and Biesheuvel (2007) who reported a similar frequency for particles both the Low and High-Frequency Regimes and was interpreted as a possible fourth harmonic of the Low-Frequency $f^{*} = 0.07$.

When Ga is increased to the range $(215, 221)$, the trajectories lose any significant spectral signature. Neither the parallel, nor the perpendicular velocity PSD in Fig. 7(b) show any marked peak. Only a mild peak at $f^{*} = (0.01 \pm 0.01)$ is present for both parallel and perpendicular velocities and a mild peak at $f^{*} = (0.19 \pm 0.01)$, with an intensity 6 times smaller than in the previous Ga range for the parallel velocity. The angular and planarity analysis in the previous Subsection suggest that trajectories of $\Gamma \approx 7.9$ particles in this range of Ga might fall in the Planar or Rotating Regime, with some evidence of the existence on helicoidal trajectories in this regime. The estimated pitch of the helicoids ($\approx 500 d_{p}$) would correspond to a frequency of oscillation of $f^{*} = v^{*}_{\parallel}/(500) \approx 0.002$, in principle out of reach of the 0.01 resolution of the present spectral analysis. The mild peak at $f^{*} \approx 0.01$ might however be a reminiscence of this slow helicoidal motion.

At higher Ga, in the range Ga $\in (225, 235)$, the perpendicular velocity fluctuations PSD presented in Fig. 7(c) have a marked peak at the frequency $f^{*} = (0.055 \pm 0.010)$ with a broad base extending towards lower frequencies, down to the spectral resolution of 0.1. This behavior is similar to the one reported by Raaghav et al. (2022) for particles with density ratio $\Gamma \approx 3.9$ at Ga ~ 210, where a peak at $f^{*} \simeq 0.05$ and a peak at $f^{*} \simeq 0.005$ were reported. This was interpreted as a probable superposition of Low-Frequency oblique oscillations and a slow helical rotation. This scenario is consistent with the combined analysis of angle, planarity and spectral content in the present study. Indeed Fig. 4(a) shows that trajectories in the range Ga $\in (225, 235)$ are oblique, while Fig. 5 indicates coexistence of planar and non-planar (hence compatible with helical motion) trajectories in this range of Ga. Intriguingly while both, Raaghav et al.'s and the present experiments seem to observe this co-existence of Low-Frequency Oblique and helicoidal trajectories for high density ratio particles, such a behavior has not been reported in numerical simulations by Zhou and Dusek (2015).

At the largest Ga explored, Fig. 7(d) presents the PSDs for the case Ga = 235. It does not present any dominant frequency, as it is expected for Chaotic dynamics.

Overall, our study of oscillations for the high density ratio particles ($\Gamma \approx 7.9$), is in good agreement with numerical simulations apart from the range Ga $\in (227, 233)$ where Low-Frequency oscillations, possibly co-existing with non-planar helical motion, were observed but not reported in simulations. Reasonable agreement is also found with
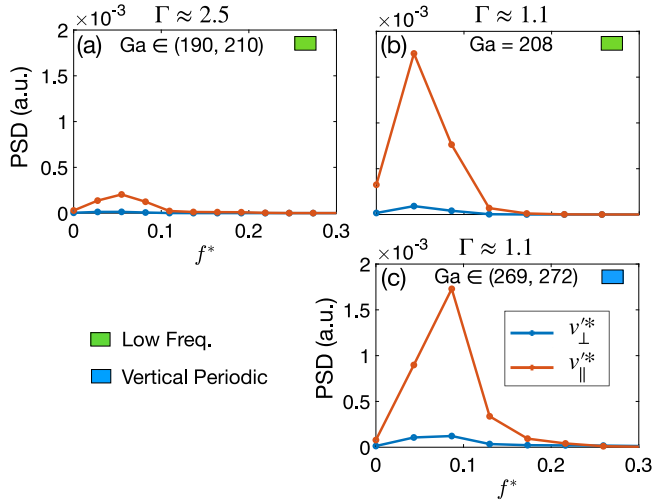
Fig. 8. PSD of parallel and perpendicular dimensionless velocity fluctuations ($v'^{*}_{\parallel}$ and $v'^{*}_{\perp}$, respectively) for $\Gamma \approx 2.5$ particles in the LF-Oblique Oscillating Regime (a) and Vertical Periodic Regime (b) and (c) for $\Gamma \approx 1.1$ particles in the LF-Oblique Oscillating Regime.

previous experiments by Raaghav et al. at density ratio $\Gamma \approx 3.9$, although we do confirm the existence of the High-Frequency oscillating region for $\mathrm{Ga} \in (187, 205)$, which they did not observe, but is predicted by the simulations by Zhou and Dusek (2015). We do not observe however the same regimes as in the study by Veldhuis and Biesheuvel (2007) at $\Gamma \approx 2.5$; in particular in the Oblique Oscillating Regimes, they report a Low-Frequency behavior (at $f^{*} \approx 0.07$) rather than a High-Frequency one, as predicted by the simulations. It is likely that is due to the fact that the density ratio they considered is very close to the Low/High-Frequency transition, found to occur around $\Gamma \approx 2.3$ in the simulations.

Fig. 8 presents PSDs of velocity fluctuations for $\Gamma \approx 1.1$ and $\Gamma \approx 2.5$ Particles, at different values of the Galileo number corresponding to the following data sets: $l^{*}_{\max} = 23.3$ for $\Gamma \approx 2.5$ particles; and $l^{*}_{\max} = 11.6$ for $\Gamma \approx 1.1$ particles. Both parallel and perpendicular components of velocity fluctuations have been analyzed. Each sub-figure presents the ensemble average of all the PSDs in the following Ga regimes: $\Gamma \approx 2.5$ Particles in the L-F Oscillating Regime showed in Fig. 7(a); and $\Gamma \approx 1.1$ Particles in the L-F Oscillating and Vertical Periodic Regimes, presented in Fig. 8(b) and (c), respectively.

The perpendicular velocity fluctuations PSDs presented in Fig. 8(b) show that for $\mathrm{Ga} = 208$ oscillations have a broad frequency peak centered around a dominant frequency $f^{*} = (0.043 \pm 0.021)$. While the parallel velocity presents a peak at the same frequency but with 10 times less energy. Note that the uncertainty is considerably higher here since the trajectories are shorter ($l^{*}_{\max} = 11.6$ or 23.3). The dominant frequency confirms the Low-Frequency nature of the oscillations qualitatively identified in the velocity signal shown in Fig. 6. This is also in agreement with the frequency predicted by numerical simulations by Zhou and Dusek (2015) and observations from Veldhuis and Biesheuvel (2007).

On the other hand, Fig. 8(c) presents the perpendicular and parallel velocity PSDs of $\Gamma \approx 1.1$ particles in the range $\mathrm{Ga} \in (269, 272)$. We observe a single broad frequency peak centered around $f^{*} = (0.085 \pm 0.021)$, that overlaps with the Low-Frequency. As for the sub-figure (a), the parallel velocity presents a peak at the same frequency but with 10 times less energy. This peak is at frequencies slightly lower than the frequency identified by Zhou and Dusek (2015) for the vertical periodic regime (of the order of $f^{*} \approx 0.15$). Overall, given the small (although not strictly zero) angle previously reported for particles in this range of parameters, our observations are globally consistent with

the existence of such a Vertical Periodic Regime. It is worth noting that the experiments of Raaghav et al. also measured non-strictly-zero angles of $0.3°$ for similar range of parameters. Raaghav et al. have measured a frequency of $f^{*} = 0.15$ very close to the numerical prediction by Zhou and Dušek. Besides they have shown that in this region of the parameters space both Chaotic and Vertical Oscillating trajectories may co-exist. This may be a possible explanation for the broader than expected peak at lower frequency here measured; given the low spectral resolution of the present measurements (for this particular dataset) we might actually be seeing a combination of Chaotic (broad spectra) and Vertical Periodic trajectories (with, a priori, $f^{*} = 0.15$).

Finally, Fig. 8(a) presents the perpendicular and parallel velocity PSDs of $\Gamma \approx 2.5$ particles in the range $\mathrm{Ga} \in (190, 210)$. The perpendicular velocity fluctuations PSD presented in Fig. 8(c) shows that oscillations have a broad frequency peak centered around a dominant frequency $f^{*} = (0.054 \pm 0.013)$. Additionally, note that, as the trajectories are longer than for $\Gamma \approx 1.1$ ($l^{*}_{\max} \in (33.3, 100)$), the uncertainty in this case is smaller (though still larger than for $\Gamma \approx 7.9$). This spectral content is in agreement with the Low-Frequency Regime predicted in numerical simulations by Zhou and Dusek (2015), and what Veldhuis and Biesheuvel (2007) have measured for particles in this area of the parameters space. A difference with the experiments of Veldhuis and Biesheuvel (2007) is however seen as they have found harmonic contributions at around $f^{*} = 0.27$ (Veldhuis and Biesheuvel, 2007).

3.5. Settling velocity & drag

In this last section we investigate the terminal settling velocity of the particles which results from the balance of the drag force and net gravity (i.e. gravity plus buoyancy). The measure of terminal velocity therefore allows to estimate the drag coefficient of the falling spheres and compare it to tabulated values for fixed spheres.

As previously discussed, the dimensional analysis of the problem of a sphere falling in a quiescent viscous fluid, yields two dimensionless control parameters: $\mathrm{Ga} - \Gamma$. When addressing the further question of the terminal vertical velocity v_s, an additional dimensionless parameter emerges: the terminal particle Reynolds number $\mathrm{Re}_{\mathrm{p}} = v_s d_p / \nu$. It is important to note that Re_{p} is a response parameter of the problem which depends on the control parameters Γ and Ga (we shall write then $\mathrm{Re}_{\mathrm{p}}(\mathrm{Ga}, \Gamma)$), therefore implying a possible impact of the path instabilities (which depend on both Ga and Γ) previously discussed on the terminal velocity of the spheres. Similarly, when it comes to address the question of the drag force experienced by the falling sphere, this introduces another dimensionless parameter, the drag coefficient C_D, which shall also be considered a priori as a function of both Ga and Γ (we shall write $C_D(\mathrm{Ga}, \Gamma)$). This situation therefore contrasts with the case of the drag force of a fixed sphere in a prescribed mean stream, as in that situation, the density ratio is not a relevant parameter, and Reynolds number is then the unique control parameter of the problem. The drag coefficient solely depends in that case on the sphere Reynolds number $C_D(\mathrm{Re}_{\mathrm{p}})$.

This then raises several points for the case of settling spheres:

(i) Are the usual correlations for the drag coefficient $C_D(\mathrm{Re}_{\mathrm{p}})$ (not explicitly dependent on the density ratio Γ) still valid for the case of falling spheres (where Re_{p} and C_D may have explicit dependencies on both Ga and Γ)? Recall that explicit dependency on density ratio is known to be potentially major for light particles with $\Gamma \ll 1$ (Auguste and Magnaudet, 2018; Karamanev and Nikolov, 1992);

(ii) Re_{p} being a response parameter, usual correlations for the drag coefficient of fixed spheres $C_D(\mathrm{Re}_{\mathrm{p}})$ are impractical as Re_{p} is not known beforehand: correlations directly implying the actual control parameters (Ga, Γ) (eventually only Ga if explicit dependency on density ratio is found not to be important) would be more practical;

(iii) If density ratio is found to play a role, how important are the associated effects?

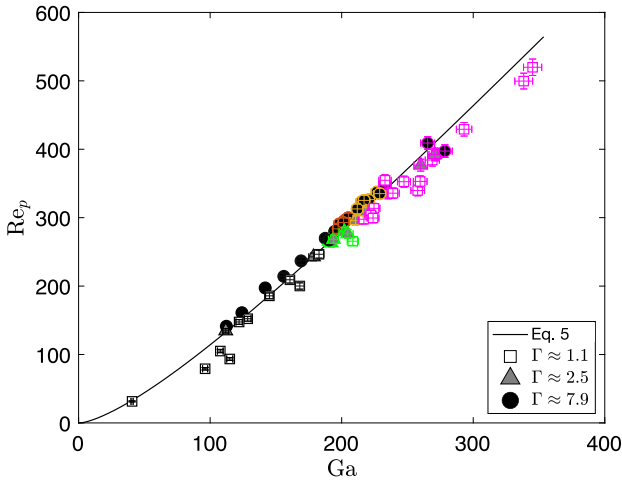We address here these questions.

Fig. 9. Galileo number versus particle Reynolds number alongside with the empirical correlation from Eq. (5). The symbols represent the different density ratios (i.e. particle material): squares — $\Gamma \approx 1.1$; triangles — $\Gamma \approx 2.5$; circles — $\Gamma \approx 7.9$. Whereas the edge colors represent the different trajectory regimes, as in Fig. 2: black — Rectilinear & Oblique; green — Low-Freq.; orange — High-Freq.; yellow — Planar or Rotating; and magenta — Chaotic & Vertical Periodic.

3.5.1. New correlation relations between Galileo number and terminal particle Reynolds number/Drag coefficient

Consider a settling particle within a given point of the parameters space (Ga, Γ), with a terminal settling velocity $v_s(Ga, \Gamma)$. From the definition of the terminal particle Reynolds number $Re_p = v_s d_p/\nu$ and of the Galileo number $Ga = U_g d_p/\nu$, we can define the dimensionless particle terminal velocity v_s^*, which can be rewritten in terms of Ga and Re_p (Cabrera, 2022):

$$v_s^*(Ga, \Gamma) = \frac{v_s}{U_g} = \frac{Re_p(Ga, \Gamma)}{Ga}. \tag{2}$$

Regarding drag, considering that in the terminal settling the drag force $F_D = \frac{1}{8}\rho_f C_D \pi d_p^2 v_s^2$ equals the gravity-buoyancy force $F_g = \frac{\pi}{6}(\rho_p - \rho_f)d_p^3 g = \frac{\pi}{6}\rho_f d_p^2 U_g^2$, from relation (2) the drag coefficient can be simply expressed as (Cabrera, 2022):

$$C_D(Ga, \Gamma) = \frac{4}{3}\left(\frac{Ga}{Re_p(\Gamma, Ga)}\right)^2. \tag{3}$$

Note that in this expression, the particle Reynolds number $Re_p(Ga, \Gamma)$ a response parameter of the problem, which is not known *a priori* and needs to be measured. As further discussed below it can be analytically expressed only in the vanishing Galileo number limit, which corresponds to the steady vertical Stokes settling regime.

Fig. 9 presents the measurements of Re_p versus Galileo number, for all particles (of all density ratios and for all the settling regimes) explored in the present study. The points appear to be relatively well packed on a main common trend, implying a minor direct dependency of Re_p on the density ratio Γ (note that an implicit dependency on Γ still exist via $Ga = \sqrt{(\Gamma - 1)g d_p^3}/\nu$). Some scatter of the points is however visible, which may still reflect a possible explicit (minor) correction to the main trend due to the density ratio (this aspect will be further discussed in the next Subsection).

Before addressing such possible corrections, let first consider as a first approximation that Re_p is independent on the density ratio and only explicitly dependent on Ga. According to (3), that implies then that the drag coefficient C_D is itself also independent of the density ratio, and solely dependent on Ga. Since Re_p and Ga are then related, C_D can be equivalently considered as Ga-dependent or Re_p-dependent. This is in agreement with previous studies by Horowitz and Williamson (2010)

and Raaghav et al. (2022) who measured the drag coefficient of falling spheres and did not observe, within the scatter of their measurements, a significant deviation compared to the fixed sphere case.

It can be noted that the empirical finding that neither C_D nor Re_p explicitly depend on Γ, while they are univocally related via Ga, is trivial in the Stokes settling regime (in the limit of vanishing Ga and Re_p). In this limit, analytical solutions of Stokes equations, lead indeed to $C_D(Re_p) = 24/Re_p$, that combined with Eq. (3) yields $Re_p = \frac{1}{18}Ga^2$.

For non vanishing Ga and Re_p, a univoque relation between Re_p and Ga supports then the idea that an explicit correlation $Re_p(Ga)$ between these two parameters (via (6)) can be derived using classical correlations for $C_D(Re_p)$ for fixed spheres. We propose here to use the correlation by Brown and Lawler (2003), which accurately fits the drag coefficient for spheres over a broad range of Reynolds number (up to $Re_p \lesssim 2 \times 10^5$):

$$C_D(Re_p) = \frac{24}{Re_p}(1 + 0.150 Re_p^{0.681}) + \frac{0.407}{1 + \frac{8710}{Re_p}}. \tag{4}$$

By including this expression of $C_D(Re_p)$ into (3), we can indeed provide a direct correlation for the terminal particle Reynolds number (and hence for the particle terminal velocity) only depending on the actual control parameter of the problem which is the Galileo number:

$$Re_p^{\dagger}(Ga) = \frac{Ga^2(22.5 + Ga^{1.364})}{0.0258Ga^{2.6973} + 2.81Ga^{2.0306} + 18Ga^{1.364} + 405}. \tag{5}$$

This expression is represented in Fig. 9 by the solid line, and is found in very good agreement with the global trend measured for the settling particles in our experiments (what essentially confirms that the drag coefficient for fixed spheres reasonably applies to the case of falling spheres). Beyond this agreement, the above correlation is of great practical interest as it allows a direct determination of the settling velocity of a sphere from the sole *a priori* knowledge of its Galileo number (which is a true control parameter, only requiring to know the particle-to-fluid density ratio, the sphere diameter, the acceleration of gravity and the ambient fluid's kinematic viscosity), without the need of using the traditional $C_D(Re_p)$ correlation to solve (numerically) the non-linear equation (3): $Re_p^2 C_D(Re_p) = \frac{4}{3}Ga^2$.

Similarly, a direct correlation between the drag coefficient and the actual control parameter of problem (Ga) (rather than the usual correlation $C_D(Re_p)$, which connects two response parameters) can be derived by re-introducing expression (5) back into (3):

$$C_D^{\dagger}(Ga) = \frac{4}{3}\left(\frac{0.0258Ga^{2.6973} + 2.81Ga^{2.0306} + 18Ga^{1.364} + 405}{Ga(22.5 + Ga^{1.364})}\right)^2. \tag{6}$$

3.5.2. Density ratio effect

The new correlations (5) and (6) we just proposed assume that both the terminal Reynolds number Re_p and the drag coefficient C_D only depend on Ga and do not depend explicitly on Γ. Based on Fig. 9, this seems a reasonable global assumption, though some scatter of the points in Fig. 9 and small deviations (in particular for the less dense particles, $\Gamma \approx 1.1$ particles, represented as squares in the figure) with respect to relation (5) cannot rule out a possible (minor) effect of density ratio.

To better test possible deviations due to density ratio effects, we show in Figs. 10 and 11 the terminal Reynolds number and the drag coefficient compensated respectively by relations (5) and (6) such that a value of zero would correspond to a perfect match (hence with no density effects).

Fig. 10 (for the compensated terminal Reynolds number) shows that although the measurements for all different datasets obtained in this work are indeed distributed around zero, they can deviate from this density-independent trend with a scatter of typically $\pm 10\%$. More importantly it can be seen that (apart for two outliers out of the 68 independent measurements we carried) the scatter of the points present
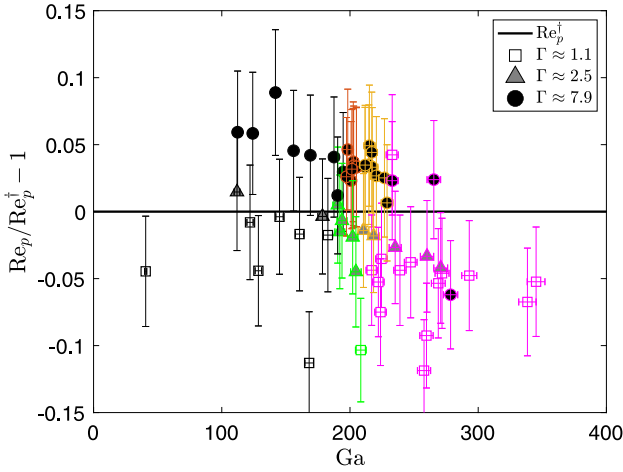
Fig. 10. Galileo number versus particle Reynolds number compensated by the empirical correlation from Eq. (5). The symbols represent the different density ratios (i.e. particle material): squares — $\Gamma \approx 1.1$; triangles — $\Gamma \approx 2.5$; circles — $\Gamma \approx 7.9$. Whereas the edge colors represent the different trajectory regimes, as in Fig. 2: black — Rectilinear & Oblique; green — Low-Freq.; orange — High-Freq.; yellow — Planar or Rotating; and magenta — Chaotic & Vertical Periodic.
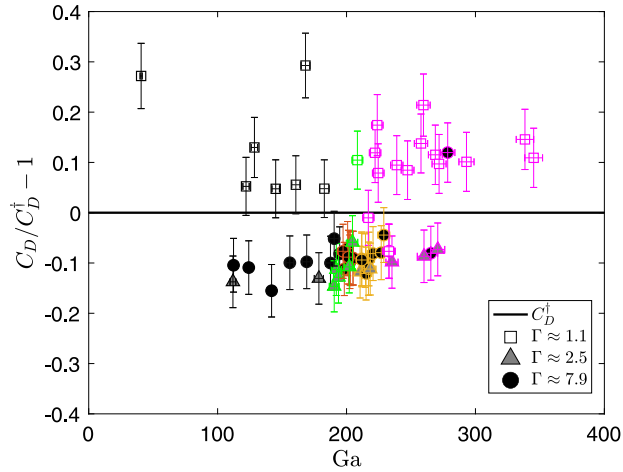
Fig. 11. Drag coefficient compensated by the empirical correlation from Eq. (6) versus Galileo number. The symbols represent the different density ratios (i.e. particle material): squares — $\Gamma \approx 1.1$; triangles — $\Gamma \approx 2.5$; circles — $\Gamma \approx 7.9$. Whereas the edge colors represent the different trajectory regimes, as in Fig. 2: black — Rectilinear & Oblique; green — Low-Freq.; orange — High-Freq.; yellow — Planar or Rotating; and magenta — Chaotic & Vertical Periodic.

a systematic trend with the density ratio, where less dense particles (notably $\Gamma \approx 1.1$ particles and, to a less extent, $\Gamma \approx 2.5$ particles) are systematically below the correlation derived from fixed spheres, while heavy particles are systematically above. The density-independence approximation seems therefore to give a reasonable average trend to predict the terminal Reynolds number using relation (5) though denser particles will have a positive bias (settling up to 10% faster in the range of densities explored here) and lighter particles a negative bias (up to 13% slower in the range of densities explored here).

Similarly Fig. 11 shows that (apart for the same two outliers out of the 68 independent measurements we carried), a systematic effect of density ratio can be observed on the drag coefficient C_D, where less dense particles (notably $\Gamma \approx 1.1$ particles) have a systematic positive bias (i.e. their drag coefficient is larger, up to + 15% in the range of densities we explored) compared to the correlation derived from fixed spheres, while heavy particles have systematic negative bias (i.e. their drag coefficient is lower, up to −15% in the range of densities we

explored) compared to the correlation derived from fixed spheres. The overall drag coefficient spread is 30%.

These results challenge the widespread idea that the drag coefficient (and eventually then its connection to the terminal settling velocity via relation (6)) of freely settling spheres (i.e. with $\Gamma > 1$) do not explicitly depend on the density ratio Γ. Previous studies are however not in contradiction with this claim (Auguste and Magnaudet, 2018; Horowitz and Williamson, 2010; Raaghav et al., 2022; Veldhuis and Biesheuvel, 2007). Indeed, while these studies did not specifically focus on a quantitative estimation of possible fine deviations from the fixed sphere case, small systematic deviations can actually be observed in the reported data. In particular, we find a systematic explicit dependence on Γ, as C_D and Re_p vary in 25% to 30% between the less dense ($\Gamma \approx 1.1$) and the denser particles ($\Gamma \approx 7.5$). It is worth to remark that the results from the denser particles ($\Gamma \approx 7.9$ particles) and the intermediate density ratio ones ($\Gamma \approx 2.5$ particles) are hardly distinguishable (in particular regarding the drag coefficient in Fig. 11). This suggests that the Γ dependency might be most relevant for Γ values close to one, i.e. closer to the rising particle case where a clear dependency with Γ was reported for the drag coefficient (Karamanev and Nikolov, 1992; Auguste and Magnaudet, 2018) and has been found to be systematically larger compared to the case of fixed spheres. Deviations for light particles with $\Gamma \lesssim 1$ remain small and comparable to the ones we report here for $\Gamma \approx 1.1$ particles with $\Gamma \gtrsim 1$, and become important for very light spheres with $\Gamma \ll 1$.

4. Conclusions

We presented in this article an experimental study on the settling of single spheres in a quiescent flow, with a systematic characterization of settling regimes, settling terminal velocity and drag coefficient of spheres with density ratios up to $\Gamma \simeq 8$ (previous similar studies were limited to $\Gamma < 4$). The spheres dynamics is analyzed in the parameters space Γ – Ga, with particle-to-fluid density ratios $\Gamma \in (1.1, 7.9)$ and Galileo numbers Ga $\in (100, 340)$.

Overall, our results on the settling regimes are in very good agreement with the numerical simulations by Zhou and Dusek (2015) and in partial agreement with previous experiments by Veldhuis and Biesheuvel (2007) and Raaghav et al. (2022) over a narrower range of density ratios.

In particular, we confirm that for all situations, trajectories eventually become chaotic in the high Galileo number limit (typically for Ga > 250) although the details of the route to chaos depends on the density ratio of the particles. For the lowest density ratio, we observe all the regimes predicted by Zhou and Dusek (2015) simulations. In particular we confirm the Low-Frequency nature of Oblique Oscillating Regime (for Ga $\lesssim$ 200 for $\Gamma = 1.1$ and around Ga $\approx$ 200 for $\Gamma = 2.5$) with a dominant dimensionless frequency $f^* \approx 0.06$. While this regime (predicted by Zhou and Dusek (2015)) was reported by Raaghav et al. (2022), it was not clearly observed in experiments by Veldhuis & Biesheuvel. We also confirm that particles with density ratio close to unity (Plastic Particles with $\Gamma = 1.1$) exhibit a "pocket" of vertical periodic settling in the range Ga $\in (250, 300)$. This regime predicted in simulations by Zhou and Dusek (2015) was also reported in experiments by Raaghav et al. although it was not observed by Veldhuis & Biesheuvel.

For the densest particles we investigated (Metallic Particles with $\Gamma = 7.9$), which are also the densest reported for such experimental studies, we confirm the existence of a High-Frequency Oblique Oscillating Regime, around Ga $\approx$ 200 with $f^* \approx 0.18$. This regime was not observed in experiments Raaghav et al. (2022) at $\Gamma = 3.9$ who only reported helical/rotating trajectories. We also observe such helical trajectories (around Ga $\approx$ 220), which we find to co-exist with the High-Frequency Oblique Oscillating Regime for Ga $\lesssim$ 220, in agreement with what Zhou and Dusek (2015) identified as a multi-stable Planar-or-Rotating Regime, where both planar (oblique oscillating trajectories)

and non-planar (helical trajectories) could be observed. We find however that the range of multi-stability is probably larger than what is reported in the numerical study by Zhou and Dusek (2015), as helicoids were randomly observed over almost the entire range of Galileo numbers *a priori* corresponding to the High-Frequency Oblique Oscillating Regime. This may explain why the High-Frequency Oblique Oscillating Regime was not reported in Raaghav et al. (2022), who may have only (randomly) observed helical trajectories in this range. Concerning the helical trajectories, although the limited extent of the measurement volume in our experiment did not allow to fully characterize the helical properties, raw estimates of the radius (about 7 particle diameters) and the pitch (several hundreds particle diameters) of the portion of helicoids we observed are consistent with previous values reported in experiments by Raaghav et al. (2022) and simulations by Zhou and Dusek (2015).

Finally, our study of the spheres terminal settling velocity (v_s) and drag coefficient C_D carries two important results. First, neglecting density ratio dependencies, we have proposed two new correlations directly relating the terminal Reynolds number $\mathrm{Re}_p = v_s d_p / \nu$ and the drag coefficient C_D to the Galileo number Ga. For the case of settling spheres, these relations are more handy to use compared to classical correlations between the C_D and Re_p as, contrary to Ga which is a true control parameter of the problem, Re_p is a response parameter which cannot be determined beforehand. Secondly, we have shown that the usual approximation to neglect an explicit dependency on the density ratio Γ (other than the implicit dependency through Ga of the terminal Reynolds number and drag coefficient) for settling spheres is not justified from the dimensional analysis and not fully supported by experimental findings. In particular, a trend was observed were the drag coefficient of the lightest particles was systematically larger than for the densest particles, with a difference up to about 30% over the entire range of parameters we investigated. This indicates that, at least in the range of Galileo numbers explored here (with rich and complex settling regimes), while using the drag coefficient from usual correlations tabulated for fixed spheres (which can be considered as infinitely dense) at the corresponding Reynolds number may give the good order of magnitude of the terminal velocity, an accurate estimate would require to account for finite density ratio effects. Beyond the case of spheres settling in quiescent fluid addressed here, such corrections may also play a role in the context of modeling the drag force coupling of finite size inertial particles advected and settling in turbulent flows.

Declaration of competing interest

The authors declare that they have no known competing financial interests or personal relationships that could have appeared to influence the work reported in this paper.

Data availability

Data will be made available on request.

Acknowledgments

References

Aliseda, A., Cartellier, A., Hainaux, F., Lasheras, J.C., 2002. Effect of preferential concentration on the settling velocity of heavy particles in homogeneous isotropic turbulence. J. Fluid Mech. 468, 77–105.

Auguste, Franck, Magnaudet, Jacques, 2018. Path oscillations and enhanced drag of light rising spheres. J. Fluid Mech. 841, 228.

Bonnefis, Paul, Fabre, David, Magnaudet, Jacques, 2023. When, how, and why the path of an air bubble rising in pure water becomes unstable. Proc. Natl. Acad. Sci. 120, e2300867120.

Bourgoin, M., Huisman, S.G., 2020. Using ray-traversal for 3D particle matching in the context of particle tracking velocimetry in fluid mechanics. Rev. Sci. Instrum. 91, 085105.

Brown, Phillip P., Lawler, Desmond F., 2003. Sphere drag and settling velocity revisited. J. Environ. Eng. 129, 222.

Cabrera, Facundo, 2022. Settling of Particles in Quiescent and Turbulent Flows. from Ground Conditions to Micro-Gravity (Ph.D. Thesis). At the École Normale Supérieure De Lyon.

Cabrera, Facundo, Cobelli, Pablo J., 2021. Design, construction and validation of an instrumented particle for the Lagrangian characterization of flows. Exp. Fluids 62, 19.

Cabrera, F., Sheikh, M.Z., Mehlig, B., Plihon, N., Bourgoin, M., Pumir, A., Naso, A., 2022. Experimental validation of fluid inertia models for a cylinder settling in a quiescent flow. Phys. Rev. Fluids 2, 024301.

Chhabra, R.P., Agarwal, S., Chaudhary, K., 2003. A note on wall effect on the terminal falling velocity of a sphere in quiescent Newtonian media in cylindrical tubes. Powder Technol. 129, 53.

Chouippe, Agathe, Uhlmann, Markus, 2019. On the influence of forced homogeneous-isotropic turbulence on the settling and clustering of finite-size particles. Acta Mech. 230 (2), 387–412.

Ern, Patricia, Risso, Frédéric, Fabre, David, Magnaudet, Jacques, 2012. Wake-induced oscillatory paths of bodies freely rising or falling in fluids. Annu. Rev. Fluid Mech. 44, 97.

Fabre, David, Auguste, Franck, Magnaudet, Jacques, 2008. Bifurcations and symmetry breaking in the wake of axisymmetric bodies. Phys. Fluids 20, 051702.

Fabre, David, Tchoufag, Joel, Magnaudet, Jacques, 2012. The steady oblique path of buoyancy-driven disks and spheres. J. Fluid Mech. 707, 24.

Falkinhoff, F., Obligado, M., Bourgoin, M., Mininni, P.D., 2020. Preferential concentration of free-falling heavy particles in turbulence. Phys. Rev. Lett. 125, 064504.

Fornari, Walter, Picano, Francesco, Brandt, Luca, 2016. Sedimentation of finite-size spheres in quiescent and turbulent environments. J. Fluid Mech. 788, 640.

Good, G.H., Ireland, P.J., Bewley, G.P., Bodenschatz, E., Collins, L.R., Warhaft, Z., 2014. Settling regimes of inertial particles in isotropic turbulence. J. Fluid Mech. 759, R3.

Herrada, Miguel A., Eggers, Jens G., 2023. Path instability of an air bubble rising in water. Proc. Natl. Acad. Sci. 120, e2216830120.

Horowitz, M., Williamson, C.H.K., 2010. The effect of Reynolds number on the dynamics and wakes of freely rising and falling spheres. J. Fluid Mech. 651, 251.

Jenny, Mathieu, Bouchet, Gilles, Dusek, Jan, 2003. Nonvertical ascension or fall of a free sphere in a Newtonian fluid. Phys. Fluids 15 (1), L9–L12.

Jenny, M., Dusek, J., Bouchet, G., 2004. Instabilities and transition of a sphere falling or ascending freely in a Newtonian fluid. J. Fluid Mech. 201.

Karamanev, Dimitar G., Nikolov, Ludmil N., 1992. Free rising spheres do not obey newton's law for free settling. AIChE J. 38, 1843.

Maxey, M., 1987. The gravitational settling of aerosol-particles in homogeneous turbulence and random flow-fields. J. Fluid Mech. 174, 441–465.

Nakamura, Isao, 1976. Steady wake behind a sphere. Phys. Fluids 19, 5.

Natarajan, Ramesh, Acrivos, Andreas, 1993. The instability of the steady flow past spheres and disks. J. Fluid Mech. 254, 323.

Nielsen, Peter, 1993. Turbulence effects on the settling of suspended particles. J. Sediment. Res. 63 (5), 835–838.

Obligado, M., Bourgoin, M., 2022. Dynamics of towed particles in a turbulent flow. J. Fluids Struct. 114, 103704.

Ormières, Delphine, Provansal, Michel, 1999. Transition to turbulence in the wake of a sphere. Phys. Rev. Lett. 83, 80.

Ouellette, Nicholas T., Xu, Haitao, Bodenschatz, Eberhard, 2005. A quantiaive study of three-dimensional Lagrangian particle tracking algorithms. Exp. Fluids 39, 722.

Raaghav, Shravan K.R., Poelma, Christian, Breugem, Wim-Paul, 2022. Path instabilities of a freely rising or falling sphere. Int. J. Multiph. Flow 153, 104111.

Rosa, Bogdan, Parishani, Hossein, Ayala, Orlando, Wang, Lian Ping, 2016. Settling velocity of small inertial particles in homogeneous isotropic turbulence from high-resolution DNS. Int. J. Multiph. Flow.

Tomboulides, Ananias G., Orszag, Steven, 2000. Numerical investigation of transitional and weak turbulent flow past a sphere. J. Fluid Mech. 416, 45.

Tran-Cong, Sabine, Gay, Michael, Michaelides, Efstathios E., 2004. Drag coefficients of irregularly shaped particles. Powder Technol. 139, 21.

Uhlmann, Markus, Doychev, Todor, 2014. Sedimentation of a dilute suspension of rigid spheres at intermediate galileo numbers: the effect of clustering upon the particle motion. J. Fluid Mech. 752, 310.

Veldhuis, C.H.J., Biesheuvel, A., 2007. An experimental study of the regimes of motion of spheres falling or ascending freely in a Newtonian fluid. Int. J. Multiph. Flow 1074.

Zhao, Yu, Davis, Robert H., 2003. Interaction of sedimenting spheres with multiple surface roughness scales. J. Fluid Mech. 492, 101.

Zhou, Wei, 2016. Instabilités De Trajectoires De Spheres, Ellipsoides Et Bulles (Ph.D. thesis).

Zhou, W., Dusek, J., 2015. Chaotic states and order in the chaos of the paths of freely falling and ascending spheres. Int. J. Multiph. Flow 205.